JACS
JOURNAL OF THE AMERICAN CHEMICAL SOCIETY

Article

pubs.acs.org/JACS

Transition State Analysis of Enolpyruvylshikimate 3-Phosphate (EPSP) Synthase (AroA)-Catalyzed EPSP Hydrolysis

Meiyan Lou,[†] Steven K. Burger,[‡] Meghann E. Gilpin,[§,†] Vivian Gawuga,[‡] Alfredo Capretta,[‡] and Paul J. Berti*[,‡,†]

[‡]Department of Chemistry & Chemical Biology, and [†]Department of Biochemistry & Biomedical Sciences, McMaster University, 1280 Main Street West, Hamilton, Ontario L8S 4M1, Canada

Supporting Information

ABSTRACT: Proton transfer to carbon atoms is a significant catalytic challenge because of the large intrinsic energetic barrier and the frequently unfavorable thermodynamics. The main catalytic challenge for enolpyruvylshikimate 3-phosphate synthase (EPSP synthase, AroA) is protonating the methylene carbon atom of phosphoenolpyruvate, or EPSP, in the reverse reaction. We performed transition state analysis using kinetic isotope effects (KIEs) on AroA-catalyzed EPSP hydrolysis, which also begins with a methylene carbon (C3) protonation, as an analog of AroA's reverse reaction. As part of this analysis, an inorganic phosphate scavenging system was developed to remove phosphate which, though present in microscopic amounts in solution, is ubiquitous. The reaction was stepwise, with irreversible C3 protonation to form an EPSP cation intermediate; that is, an $A_H^{\ddagger}*A_N$ mechanism. The large experimental 3-^{14}C KIE, 1.032 ± 0.005, indicated strong coupling of C3 with the motion of the transferring proton. Calculated 3-^{14}C KIEs for computational transition state models revealed that the transition state occurs early during C3−H$^+$ bond formation, with a C3−H$^+$ bond order of ≈0.24. The observed solvent deuterium KIE, 0.97 ± 0.04, was the lowest observed to date for this type of reaction, but consistent with a very early transition state. The large 2-^{14}C KIE reflected an "electrostatic sandwich" formed by Asp313 and Glu341 to stabilize the positive charge at C2. In shifting the transition state earlier than the acid-catalyzed reaction, AroA effected a large Hammond shift, indicating that a significant part of AroA's catalytic strategy is to stabilize the positive charge in the EPSP cation. A computational model containing all the charged amino acid residues in the AroA active site close to the reactive center showed a similar Hammond shift relative to the small transition state models.

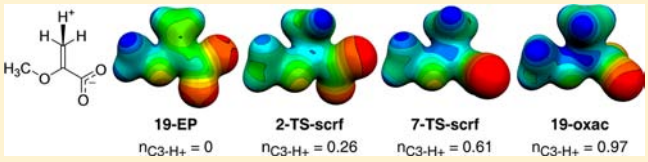

INTRODUCTION

Enolpyruvylshikimate 3-phosphate synthase (AroA,[1] also called EPSP synthase) synthesizes enolpyruvylshikimate 3-phosphate (EPSP) and phosphate (P_i) from shikimate 3-phosphate (S3P) and phosphoenolpyruvate (PEP) (Scheme 1) as part of the shikimate biosynthetic pathway in bacteria, plants, and some parasites.[2,3] AroA is a potential antibacterial target, as knockout strains are avirulent.[4] In plants, it is the target of the herbicide glyphosate (*N*-(phosphonomethyl)glycine).[5] Its only homologue, MurA, is also a carboxyvinyl transferase and part of the peptidoglycan biosynthetic pathway in bacteria. It is the target of the antibiotic fosfomycin.[6]

AroA and MurA have been the targets of antibiotic development for four decades, but inhibitor design remains challenging. The reaction proceeds through an addition/elimination pathway involving a tetrahedral intermediate (THI). The THI has been targeted with mimics, and some potent inhibitors have been created.[7,8] However, the THI is not necessarily a good target for inhibitor design, as AroA *destabilizes* the THI, accelerating its breakdown 10^5-fold relative to solution.[9] Rather, AroA stabilizes the transition states (TSs) for THI formation and breakdown.[10] These are the species to which the enzyme should bind most tightly. Determining the TS structure by TS analysis therefore represents a step toward creating potent AroA inhibitors.

In this study, we performed TS analysis using multiple kinetic isotope effects (KIEs) to determine the TS structure.[11−13] KIEs report on changes in molecular structure between the reactant and transition states, as well as atoms' movement in the reaction coordinate. The "reaction coordinate contribution" arises from the normal vibrational mode with an imaginary frequency (sometimes written as a negative frequency) which describes the atoms' movements through the transition state from reactants to products.[14] The "structural contribution" largely reflects changes in bond strengths. A bond becoming weaker at the transition state will give a normal (>1) structural contribution, while a stronger bond gives an inverse (<1) structural contribution. The overall KIE reflects both structural and reaction coordinate contributions.

AroA-catalyzed EPSP hydrolysis was chosen for TS analysis because the first step, protonating C3 to form the EPSP cation (Scheme 1), is the same as in the overall reverse reaction of EPSP + P_i → S3P + PEP. This step is the main catalytic

Received: May 4, 2012
Published: July 5, 2012

   dx.doi.org/10.1021/ja304339h | *J. Am. Chem. Soc.* 2012, 134, 12958−12969

Scheme 1

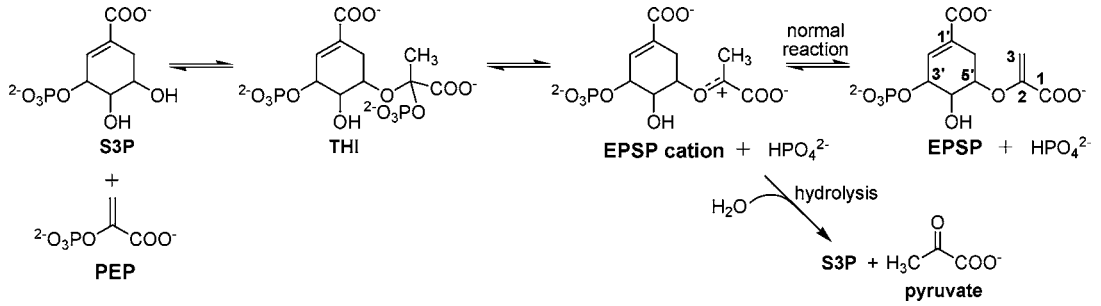

imperative for AroA; that is, it is the most difficult catalytic step. TS analysis requires that one step be cleanly irreversible, but every step of the normal AroA reaction is reversible.[15,16] We show in this study that C3 protonation is the first irreversible step in EPSP hydrolysis, making it amenable to TS analysis. We reported the TS analysis of acid-catalyzed EPSP hydrolysis in the accompanying publication.[17] Compared with the acid-catalyzed reaction, AroA accomplishes a large Hammond shift, forming an earlier transition state. This suggests that AroA's primary catalytic strategy is to stabilize the positive charge of the oxacarbenium ion intermediate.

MATERIALS AND METHODS

General. All reagents were purchased from Sigma-Aldrich or Bioshop Canada (Burlington, ON) except as noted. His-tagged *E. coli* AroA and S3P were prepared and assayed as described previously.[16,18] Radiolabeled EPSPs were synthesized as described in the accompanying publication.[17]

EPSP Hydrolysis. AroA-catalyzed EPSP hydrolysis reactions contained 50 μM AroA and 500 μM EPSP in 50 mM Tris·Cl, pH 7.5, plus a P_i scavenging system (see below). Aliquots (50 μL) were removed at time points up to 6 h and mixed with 150 μL of 0.3 M KOH to quench the reaction. Denatured protein was removed by centrifugal ultrafiltration over Microcon YM10 membranes (Millipore Corp.) at 14,000*g* for 1 h. The extent of reaction was determined by anion exchange HPLC of 150 μL of filtrate under the same conditions as for EPSP purification, using the ε_{240} ratio for S3P/PEP/EPSP of 0.59:1.0:2.1.[19]

Phosphate Scavenging System. Free P_i in solution would have confounded experiments to measure solvent deuterium incorporation into EPSP by allowing EPSP and P_i to react to reversibly form S3P and PEP, resulting in incorporation of one solvent deuteron in each catalytic cycle. A P_i scavenging system was developed to exhaustively remove free P_i from solution (Scheme 2). Reaction mixtures contained

Scheme 2

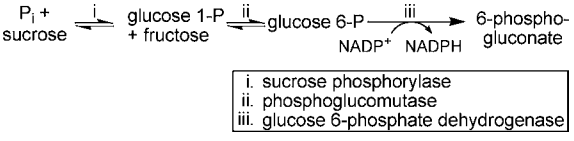

1 mM sucrose, 0.2 mM NADP, with 10 U/mL sucrose phosphorylase, 10 U/mL phosphoglucomutase, and 10 U/mL glucose 6-phosphate dehydrogenase in 50 mM Tris·Cl, pH 7.5, 50 μM KCl, and 50 μM $MgCl_2$. EPSP and AroA were incubated separately in the P_i scavenging solutions for 45 min at 37 °C before being combined to start the reaction. The P_i concentrations were far too small to detect by the conventional Malachite Green/ammonium molybdate colorimetric assay,[20] so ultimately, it was suppression of hydron exchange in EPSP that demonstrated that [P_i] had been sufficiently decreased to allow k_{ex} to be measured (see Results).

P_i scavenging with other coupled reactions failed to suppress deuterium exchange. P_i was converted in sequential reactions to PEP with AroA and EPSP (in ^1H_2O) and then to ATP with pyruvate kinase and ADP, followed by glucose 6-phosphate with hexokinase and glucose, and then 6-phosphogluconate with glucose 6-phosphate dehydrogenase and NADP. All combinations of these reactions gave $k_{ex}/k_{hyd} \geq 10$ in 50% ^2H_2O, regardless of concentrations and pretreatment times. Presumably one of the enzymes, or a contaminant, was slowly hydrolyzing one of the phosphate-containing compounds.

Solvent Deuterium KIE Measurement. The solvent deuterium KIE (SDKIE) of AroA-catalyzed EPSP hydrolysis was determined from the reaction rates in H_2O and D_2O. The reaction mixture contained 50 μM AroA, 500 μM EPSP, 50 mM Tris·Cl, pL 7.5, and the P_i scavenging system. For the D_2O reaction, Tris and the P_i scavenging system were dissolved directly in D_2O, and pD was adjusted with DCl or NaOD. EPSP was exchanged into D_2O by lyophilization, while AroA was exchanged into D_2O by gel filtration using G25 spin columns (GE Healthcare). The column was pre-equilibrated with D_2O buffer, 50 μL aliquots of AroA were applied, the columns were centrifuged at 735*g* for 2 min, and the eluted AroA was quantified by A_{280}. Residual ^1H in the D_2O solutions, as monitored by ^1H NMR, was 1.6%, a negligible amount. EPSP and AroA were incubated separately in P_i scavenging solutions at 37 °C for 45 min before being mixed together to start EPSP hydrolysis. Reactions in H_2O were prepared and run identically. EPSP hydrolysis was quantified as described above. The observed rates were equal to V_{max} because [EPSP] $\gg K_M$; therefore, SDKIE = $^HV_{max}/^DV_{max}$.

Solvent Deuterium Incorporation. Solvent ^2H incorporation into unlabeled EPSP was monitored in order to test whether C3 protonation was the first irreversible step in EPSP hydrolysis. While ^1H incorporation into [3,3-$^2H_2$]EPSP was monitored for the acid-catalyzed reaction,[17] ^2H incorporation was monitored for the AroA reaction because it was technically simpler, and the small SDKIE for the AroA reaction would not bias the assay against detecting ^2H incorporation.

Solvent ^2H incorporation into EPSP was detected by mass spectrometry, as described in the accompanying publication, and reported as $f(^2H)$ (eq 1):

$$f(^2H) = \frac{(I_{324} + 2I_{325})}{2(I_{323} + I_{324} + I_{325})} \quad (1)$$

,where I_n represents the integration of each EPSP peak in the mass spectrum. The rate of ^2H incorporation (k_{ex}) was fitted to a first order rate equation.

P_i scavenging solution was used in order to ensure that any ^2H incorporation was due to reversible EPSP protonation rather than THI formation due to contaminating P_i. Thus, reactions were run for up to 4 h with 500 μM EPSP and 10−75 μM AroA in the P_i scavenging solution, as described above, but in 50% ^2H_2O.

Competitive KIE Measurement. Competitive KIEs were determined largely as described in the accompanying article,[17] by measuring the change in isotope ratios between unreacted EPSP (0% reaction) and residual EPSP at ∼50% reaction. For ^{14}C KIEs, ^{32}P was used as a reporter on ^{12}C at the position of interest, and the ratio r_i = $^{32}P/^{14}C$ was measured. For ^2H and ^{18}O KIEs, ^{33}P reported on the

dx.doi.org/10.1021/ja304339h | J. Am. Chem. Soc. 2012, 134, 12958−12969

isotope of interest, and ^{32}P reported on ^{1}H or ^{16}O. In that case, r_i = $^{32}P/^{33}P$.

EPSP (0.25 μCi of each radiolabel) was repurified by C18 reverse phase HPLC (3.9 × 150 mm column) using isocratic elution in 50 mM ammonium acetate, pH 6, 44 mM KCl, and 2.5 mM tetrabutylammonium sulfate (TBAS), and a flow rate of 1 mL/min. Repurified EPSP was lyophilized and redissolved in H_2O. Each reaction contained 500 μM EPSP, 50 μM AroA, and the P_i scavenging system in 300 μL of 50 mM Tris·Cl, pH 7.5. EPSP and AroA were incubated separately with the P_i scavenging solutions at 37 °C for 45 min before being mixed together to start the reaction. A 100 μL aliquot was quenched immediately by heating at 95 °C (0% reaction) while the rest was incubated at 37 °C for 50 min, until it reached ≈50% completion. The 0% and 50% aliquots were repurified by anion exchange chromatography on a Mono Q column, with the isotope ratios, extent of reaction, and KIEs calculated as described in the accompanying publication.[17]

Electronic Structure Calculations, General. Most quantum mechanical optimizations and frequency calculations were performed at the B3PW91/6-31+G** level of theory with Gaussian 03 or 09,[21] as described in the accompanying publication.[17] Solvent effects were modeled in some structures with a conductor-like polarizable continuum model (CPCM),[22] using a dielectric constant equal to water's, and UA0 atomic radii. An extra sphere was placed on the proton being transferred, and SCRF frequency calculations used numerical differentiation.[23] Constrained TS optimizations were performed at the same level of theory. KIEs and equilibrium isotope effects (EIEs) were calculated using the partition functions derived from QUIVER[24] as described in the accompanying article,[17] except the temperature was 310 K.

Constrained A_H*A_N[25,26] Transition States. In an attempt to find computational TSs with higher n_{C3-H+}[27] values than found in standard TS optimizations, constrained TS optimizations of **11-TS** and **10-TS** were performed.[28−30] Values of n_{C3-H+} were constrained at 0.25 to 0.95, and n_{H+-OA} was constrained at values calculated using eq 2:

$$n_{H+-OA} = -0.448 \ln(n_{C3-H+}) + 0.0055 \quad (2)$$

Equation 2 was an empirical relationship derived from the plot of n_{C3-H+} versus n_{H+-OA} for unconstrained TS structures (see Figure 4 of the accompanying publication).[17] Vibrational frequencies and KIEs were calculated from the constrained structures.[17] Not all constrained structures yielded reaction coordinates corresponding to proton transfer (see Results).

Electrostatic Sandwich Model. Constrained optimizations on model **29** (see Figure 5) were used to study the effect of solvation on the 2-^{14}C KIE (see Discussion). Distances from C2 to the two solvating water molecules, r_{C2-O}, were constrained to identical values from 2.2 to 3.0 Å.

AroA Active Site Model. A cluster model of AroA's active site was constructed from the *E. coli* AroA·S3P crystal structure (1G6T),[31] and EPSP from the *Mycobacterium tuberculosis* AroA·EPSP·P_i crystal structure (PDB code: 2O0Z).[32] The 2O0Z structure showed EPSP's positioning and contacts in the active site, while 1G6T provided the active site residues. The structures were superimposed, and EPSP from 2O0Z was placed in 1G6T. All other ligands were removed from 1G6T. Hydrogen atoms were added with MOLPROBITY,[33] and the suggested Asn/His/Gln flips were accepted. The active site structure was relaxed with molecular dynamics (MD) runs using AMBER.[34] The MD runs were kept short, and the backbone was restrained in order to preserve the original positions of key atoms in the active site. The FF99SB AMBER parameters were used for the protein, while ANTECHAMBER was used with the general AMBER force field (GAFF) to derive parameters for EPSP. The protein·ligand complex was minimized using a 16 Å cutoff with a 2 kcal/(mol Å^2) restraint on the backbone atoms. This was followed by 100 ps of constant energy MD using the Born implicit solvent model with a dielectric constant of 80[35] and with the same 2 kcal/(mol Å^2) restraints and a 16 Å cutoff. Finally, 100 ps of MD was run with the restraints reduced to 0.5 kcal/(mol Å^2). During both MD runs, a 20 kcal/(mol Å^2) harmonic restraint was placed on the distance between the Glu341 (E341) proton and the C3 carbon of EPSP. The quantum mechanical (QM) cluster was created using the last structure of the MD run, using atoms from every residue within 4 Å of the carboxyvinyl moiety of EPSP (K22, D313, K340, E341, R344, H385, R386), plus a few key additional residues (R27, S169, S170, S197, Y200, K411; Figure 6). To reduce the size of the system, residues hydrogen bonded to EPSP's phosphate group were replaced with waters; Arg residues were replaced with guanidinium ions; Lys residues with ammonium ions; and His residues with imidazoles. The **30-TS** and **31-TS** models of the active site were initially optimized with Gaussian 09[21] at the B3PW91/6-31G* level of theory, but with extra diffuse and polarization basis functions (6-31+G**) on the carbonyl group of E341 and the C3 of EPSP. Anchoring atoms from the surrounding residues were held fixed during the minimizations. The TS was optimized using the Bofill update[36] on the reduced surface defined by the distances between E341 Oε1 and H^+, the transferring proton, and between C3 and H^+. Vibrational frequencies were calculated for the 3-^{14}C and 3-^{12}C forms of each reactant (**32-EP**, **33-EP**) and the TS model, and from those, the 3-^{14}C KIEs were calculated.[37] KIEs for the other labeled positions were calculated using QUIVER. The similarity of the 3-^{14}C KIEs calculated using QUIVER, 1.025, and the values calculated directly from Gaussian frequency calculations, 1.027, demonstrated that the constrained optimization due to the anchoring atoms did not significantly affect the KIEs calculated by QUIVER. KIEs were also calculated with **31-EP** as the reactant model to test for any large effects arising from AroA's active site. Using **31-EP** as the reactant gave a calculated 3-^{14}C KIE of 1.027 for **31-TS**, versus 1.025 with **33-EP** as the reactant, demonstrating that the active site environment did not have any large, unanticipated effects on the molecular structure.[38] Having demonstrated that KIEs calculated for the active site computational model accurately reflected the TS structure, models **30-TS**, **31-TS**, **32-EP**, and **33-EP** were reoptimized with all atoms at the B3PW91/6-31+G** level, and these models were used for the KIE calculations reported below.

RESULTS

Solvent Deuterium KIEs. Solvent deuterium KIEs (SDKIEs) were determined noncompetitively from the ratio of reaction rates in H_2O and D_2O. Noncompetitive KIEs reflect the rate-limiting step. For the AroA-catalyzed reaction, SDKIE = 0.97 ± 0.04. This appears to be the lowest SDKIE yet reported for vinyl ether hydrolysis; the smallest previously reported SDKIE was 1.3 for acid-catalyzed prostacyclin hydrolysis.[39,40] That reaction was unusual in that it underwent intramolecular general acid catalysis by a carboxyl group. Similarly, the AroA-catalyzed reaction undergoes intramolecular (or intracomplex) general acid catalysis.[16] The small SDKIE is evidence against tunneling, as large primary ^2H KIEs are one of the common signs of quantum tunneling.[41] Similarly, there was no evidence for quantum tunneling in the acid-catalyzed reaction.[17]

First Irreversible Step. Competitive KIEs, where both isotopic labels are present in the same reaction, reflect the first irreversible step or, if there are partially irreversible steps, all steps up to the first fully irreversible step.[13] As such, it was necessary to identify the first irreversible step for EPSP hydrolysis. This was done by comparing the rate constant for EPSP hydrolysis (k_{hyd} = 1 × 10^{-4} s^{-1})[10] with that of solvent ^2H exchange into EPSP (k_{ex}), as measured by mass spectrometry. Because the overall reaction to S3P and PEP incorporates one solvent ^2H at C3 in each catalytic cycle, it was necessary to create a P_i scavenging system to remove the microscopic amounts of P_i that are present in all solutions (Scheme 2). In the absence of P_i scavenging, k_{ex}/k_{hyd} was ≫100. P_i scavenging suppressed k_{ex} without altering k_{hyd}. After an initial burst of up

to 3.6% ^{2}H incorporation, possibly due to incomplete P_i scavenging before starting the reaction, there was complete suppression of ^{2}H exchange (Figure 1). That is, $k_{ex}/k_{hyd} \approx 0$,

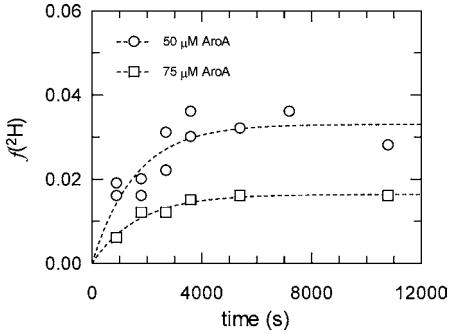

Figure 1. Solvent ^{2}H exchange into 500 μM EPSP during AroA-catalyzed hydrolysis in 50% ^2H_2O, with [AroA] = 50 or 75 μM. EPSP hydrolysis was 50% complete in ~2500 s. The dotted lines are simply a visual aid.

demonstrating that C3 protonation is irreversible in the AroA-catalyzed reaction. In all cases, the extent of ^{2}H incorporation could be neglected, even taking the burst into account.

P_i scavenging was used for the KIE measurements. For the 3,3-$^2H_2$ KIE, P_i would have caused solvent ^{1}H exchange at C3. This would have suppressed the true KIE, making a normal KIE smaller and an inverse KIE less inverse. Thus, if any exchange did occur in spite of P_i scavenging, the true 3,3-$^2H_2$ KIE would have been more inverse than the observed value of 0.990.

Competitive KIEs. Competitive KIEs were measured for every atom in the carboxyvinyl part of EPSP (Table 1, Scheme 3). ^{32}P was used as a remote label, and the $^{32}P/^{33}P$ KIE = 1.000 ± 0.004 demonstrated that there was no KIE at that position. As with acid-catalyzed EPSP hydrolysis, the 95% confidence interval for the 5′-^{18}O KIE was larger than those for other positions,[17] but the KIE was clearly inverse.

Table 1. Experimental KIEs for EPSP Hydrolysis at 310 K

isotopic label	experimental KIE[a,b]
1-^{14}C	1.005 ± 0.002 (3)
2-^{14}C	1.010 ± 0.003 (3)
3-^{14}C	1.032 ± 0.005 (3)
5′-^{18}O	0.986 ± 0.008 (3)
1,1-$^{18}O_2$	0.979 ± 0.006 (3)
3,3-$^2H_2$	0.990 ± 0.001 (3)
$^{32}P/^{33}P$[c]	1.000 ± 0.004 (3)

[a]Error is the 95% confidence interval. Number of independent trials given in parentheses. [b]^{14}C KIEs were measured using a mixture of ^{14}C and [^{32}P]EPSP. ^{32}P acted as a reporter on ^{12}C at the position of interest. ^{18}O and ^{2}H KIEs were measured by incorporating ^{33}P as a reporter radionuclide (e.g., [5′-^{18}O,^{33}P]EPSP) and were corrected for the extent of ^{18}O or ^{2}H enrichment (see Materials and Methods). [c]The $^{32}P/^{33}P$ KIE was measured as a control to test for a $^{33}P/^{32}P$ KIE at this position and for a $^{31}P/^{32}P$ KIE when ^{32}P was used as a reporter isotope in ^{14}C KIE measurements.

Competitive KIEs reflect the transition state for the first irreversible step. In the AroA reaction, the reactant state was free AroA and free EPSP in solution, while the first irreversible transition state involved C3 protonation, either on its own, or as part of a concerted addition step.

Scheme 3

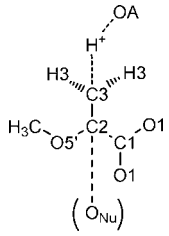

Computational TS Structures, KIEs, and EIEs. *Calculated KIEs.* KIEs were calculated for small model structures based on **1-EP** for the enolpyruvyl reactant and **1-TS** for the C3 protonation transition state. Models **25-TS** to **28-TS** were for concerted water addition (Figure 2). Oxacarbenium ion models based on **1-oxac** were used for EIE calculations. **1-oxac** itself was computationally unstable, forming an α-lactone.[17] As a result, it was necessary to include different combinations of acid catalyst, counterion, and solvating waters in the computational models. Structures were optimized in vacuo or with continuum solvation. None of the computational TS structures yielded calculated KIEs close enough to the experimental values to be considered the experimental TS, but they did establish structure/KIE relationships that made it possible to interpret the experimental KIEs. Computational TS structures were organized in terms of the Pauling bond order[27] of the C3−H$^+$ bond being formed, n_{C3-H+}. For the small models, n_{C3-H+} ranged from 0.26 (**2-TS-scrf**) to 0.77 (**11-TS**).

The reaction coordinate was predominantly a linear transfer of H$^+$ from OA to C3.[17] There were varying amounts of coupling of other atoms to this motion, as reflected in $^{light}\nu^{\ddagger}/^{heavy}\nu^{\ddagger}$, the reaction coordinate contributions (Figure 3 and Supporting Information Table S1).

The calculated 3-^{14}C KIEs were smallest for balanced transition states (i.e, n_{C3-H+} = 0.5) and increased for both early and late transition states. Some of the early TS structures had calculated 3-^{14}C KIEs within the experimental error of the experimental value, while it only reached 1.022 for the latest TS structure, **11-TS** (n_{C3-H+} = 0.77). Though there was a trend for higher 3-^{14}C KIEs at higher n_{C3-H+} values, the calculated KIEs did not reach the experimental value. The question arises then whether the true TS structure is actually later than **11-TS**. In order to discover whether an even later TS structure could be found that matched the experimental value, constrained TS optimizations were performed. There was a good match between calculated KIEs for unconstrained and constrained TS structures in the n_{C3-H+} ranges where they overlapped (Figure 4), but it was not possible to find any structure with n_{C3-H+} > 0.77 with reaction coordinates that corresponded to proton transfer. As expected, calculated 3-^{14}C KIEs for structures where there was no clear reaction coordinate for proton transfer were close to unity because the structural contribution was near unity and there was no reaction coordinate contribution (Figure 4). Thus, it was not possible to generate a very late TS model with calculated 3-^{14}C KIEs that matched the experimental value.

Constrained optimizations on model **29** were used to investigate the effect of solvation on the calculated 2-^{14}C KIE (Figure 5) (see Discussion). Distances from C2 to the two solvating water molecules, r_{C2-O}, were constrained to identical values from 2.2 to 3.0 Å.

dx.doi.org/10.1021/ja304339h | J. Am. Chem. Soc. 2012, 134, 12958−12969

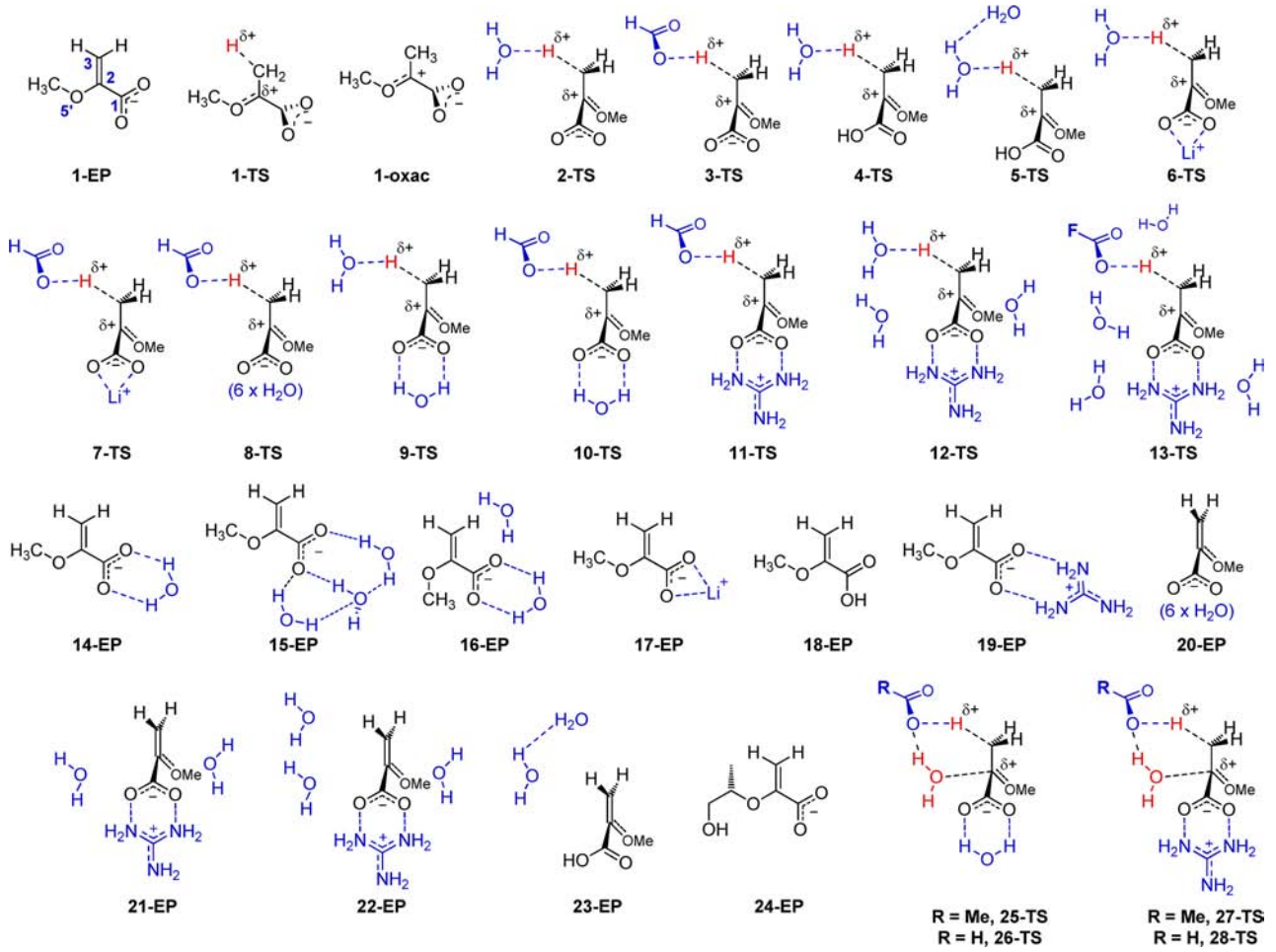

Figure 2. Computational models for IE calculations. Compound **1** is a generic model, with the suffix indicating the reactant (**EP**), transition state (**TS**), or oxacarbenium ion intermediate (**oxac**). For compounds **2**−**13**, only the **TS** models for C3 protonation are shown, though the corresponding **EP** models, and those **oxac** models that were stable, were also optimized (see Supporting Information Tables S1−S5). For compounds **14**−**24**, **EP** and some **oxac** structures were optimized. When used in the text and tables, the suffix **scrf** indicates continuum solvation (see Material and Methods). Solvating waters in compound **13** were calculated at a lower level of theory using the ONIOM methodology (see Material and Methods). Compounds **25**−**28** were for concerted protonation and water addition, i.e., an A_NA_H mechanism.

AroA Computational Model. Given the early TS structure demonstrated by the small model KIEs, the effects of the AroA active site were modeled with two cluster models, **30-TS** and **31-TS** (Figure 6). The minimal model **30-TS** had a slightly early transition state, with n_{C3-H+} = 0.40. The reaction coordinate frequency was $\nu^{\ddagger}$ = 1068*i* cm^{-1}, with $^{light}\nu^{\ddagger}/^{heavy}\nu^{\ddagger}$ = 1.002 and 3-^{14}C KIE = 1.008. Model **31-TS** included the full EPSP reactant; it had the earliest computational transition state found, with n_{C3-H+} = 0.24, $\nu^{\ddagger}$ = 935*i* cm^{-1}, $^{light}\nu^{\ddagger}/^{heavy}\nu^{\ddagger}$ = 1.008, and 3-^{14}C KIE = 1.026. The reaction coordinate frequency for **31-TS** was higher than those of small models with similar n_{C3-H+} values (Figure 3). This leads to the reaction coordinate contribution for **31-TS** being lower than those of small models with similar n_{C3-H+} values. Nonetheless, the calculated 3-^{14}C value was only moderately below the trendline because of a large structural contribution.

DISCUSSION

We showed previously that AroA forms the EPSP cation both during EPSP hydrolysis and in the normal EPSP synthesis reaction.[10] Given the nature of the experiments, however, it was not possible to demonstrate whether EPSP cation forms in every single catalytic cycle or as a rare side reaction. The pH dependence of nonenzymatic EPSP hydrolysis demonstrated that enolpyruvyl activation, i.e., C3 protonation, must occur before, or in concert with, nucleophilic attack at C2 and that C3 protonation increased the reactivity of the enolpyruvyl group by at least 5 × 10^8-fold, possibly much more. TS analysis of acid-catalyzed EPSP hydrolysis revealed a stepwise $A_H^{\ddagger}$*A_N[25,26] mechanism, with a slightly late transition state, with $n_{C3-H+} \approx$ 0.6.[17]

Possible Mechanisms. The *a priori* possible mechanisms for AroA-catalyzed EPSP hydrolysis are the same as for the acid-catalyzed reaction; and in the same way, these possibilities can be narrowed down.[17] The reaction could begin with (i) C3 protonation in a stepwise A_H*A_N mechanism, (ii) concerted C3 protonation and nucleophilic attack at C2 (A_NA_H), or (iii) unactivated nucleophilic attack at C2 in a stepwise A_N*A_H mechanism. The facts that AroA was shown by independent methods to form EPSP cation,[10] that unactivated nucleophilic attack on an enolpyruvyl group does not occur experimentally,[10] and that the EIEs of anion formation are incompatible with the experimental KIEs (Supporting Information Table S4) eliminates the last possibility. The first *irreversible* step could then be (i) or (ii) as above, or (iv) reversible C3 protonation followed by irreversible nucleophilic addition at C2, or (v) S3P

dx.doi.org/10.1021/ja304339h | J. Am. Chem. Soc. 2012, 134, 12958−12969

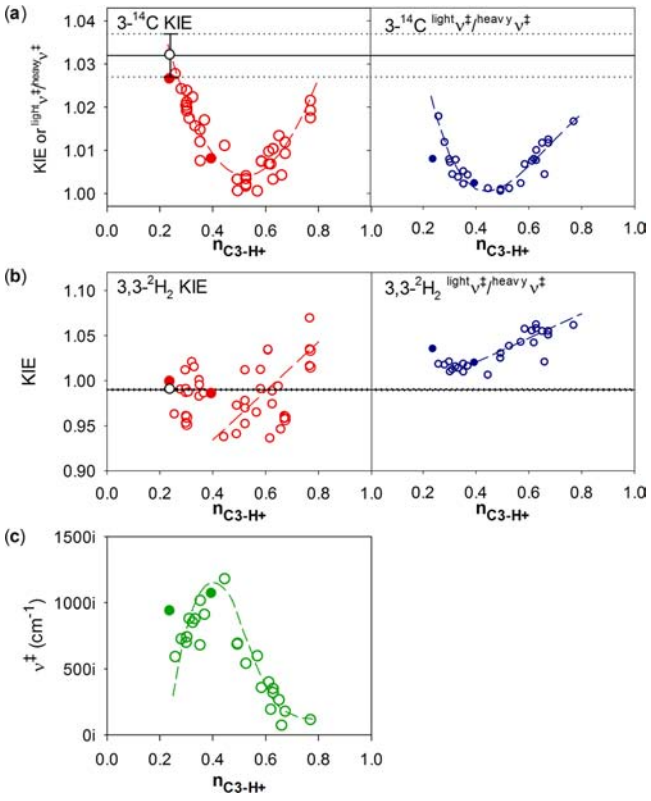

Figure 3. Calculated KIEs (left) and reaction coordinate contributions, $^{light}\nu^{\ddagger}/^{heavy}\nu^{\ddagger}$ (right) at 310 K for (a) 3-^{14}C and (b) 3,3-^{2}H$_2$, and (c) the reaction coordinate frequencies ($\nu^{\ddagger}$). The black horizontal lines represent the experimental KIE (solid line) and the 95% confidence interval (dotted lines). The calculated values for the active site models, **30-TS** (n_{C3-H+} = 0.40) and **31-TS** (n_{C3-H+} = 0.24), are shown as solid symbols. The experimental KIEs are plotted at n_{C3-H+} = 0.24, where the 3-^{14}C KIE matches the trend line. The dashed lines are intended only as visual aids. In part b, the dashed line was fitted only for points with n_{C3-H+} > 0.4. Other calculated KIEs are shown in Supporting Information Figure S1.

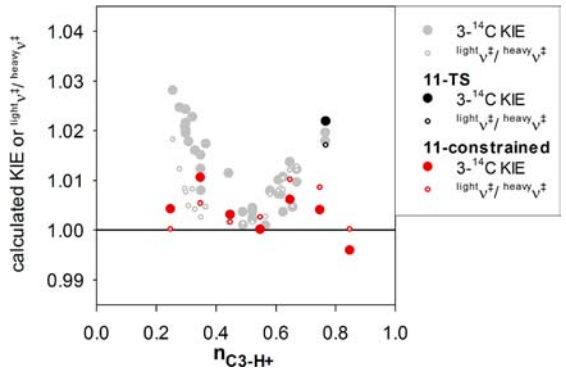

Figure 4. Calculated 3-^{14}C KIEs and reaction coordinate contributions from constrained TS optimizations. Structure **11** was optimized with n_{C3-H+} values constrained from 0.25 to 0.85 and n_{H+-OA} as defined by eq 2. Values for **11-TS** and other unconstrained TS structures are shown in black and gray, respectively. Constrained structures with n_{C3-H+} = 0.25 and 0.85 did not have any imaginary frequencies >50*i* cm^{-1}, and the imaginary frequency for n_{C3-H+} = 0.75 did not correspond to proton transfer (Supporting Information Figure S2). Essentially the same result was obtained with model **10** (Figure S3).

departure from the tetrahedral intermediate. The small k_{ex}/k_{hyd} value showed that C3 protonation was irreversible. This was

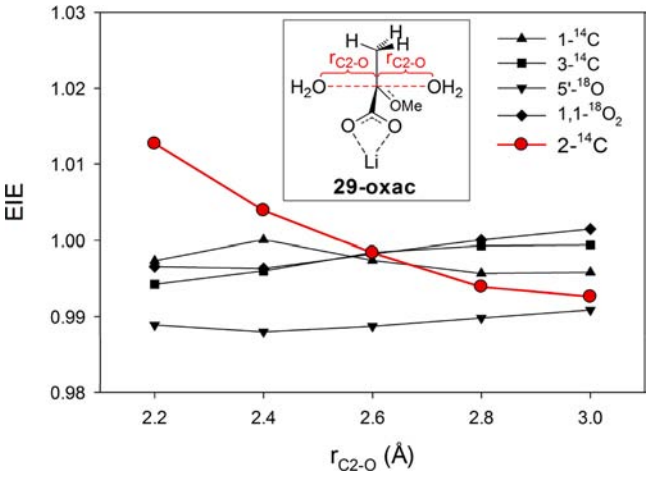

Figure 5. Model for stabilization of the cationic center at C2. Model **29** was optimized with two water molecules constrained at equal distances from C2. EIEs were calculated from the optimized structures.

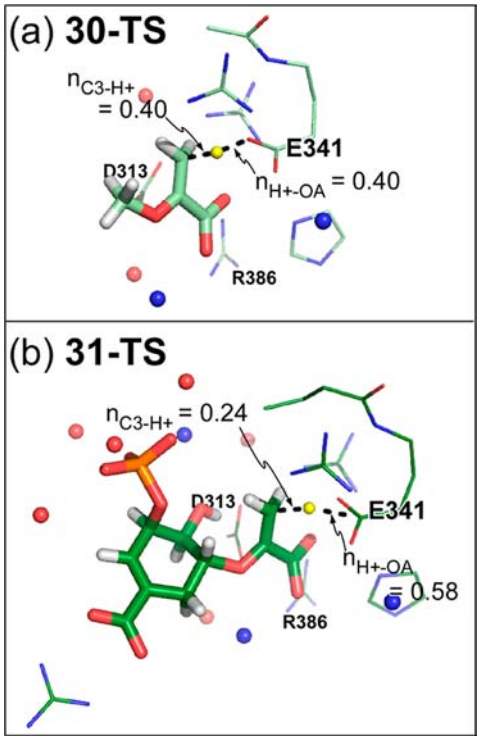

Figure 6. Cluster models of the AroA active sites (a) **30-TS** and (b) **31-TS**. The transferring proton is shown in yellow. The reactants are shown with heavy lines: enolpyruvyl methane for **30-TS** and EPSP for **31-TS**. Atoms corresponding to AroA's amino acid side chains are shown in thin lines, with the hydrogen atoms removed for clarity. The blue spheres are the ammonium ion models of Lys side chains. The proposed general acid catalytic residue, E341, is labeled, along with D313, the other residue in the proposed electrostatic sandwich,[18] and the guanidinium ion of R386, which forms a bidentate ion pair with C1. The cluster model was generated from AroA crystal structures, after a brief restrained molecular dynamics run.

consistent with the acid-catalyzed EPSP hydrolysis reaction[17] and most other enol ether functional group protonations.[42,43] The fact that it was irreversible eliminated possibilities (iv) and (v).

dx.doi.org/10.1021/ja304339h | J. Am. Chem. Soc. 2012, 134, 12958−12969

The KIEs therefore reflected either (i) C3 protonation in an $A_H^{\ddagger}*A_N$ mechanism,[25] forming the EPSP cation intermediate, or (ii) concerted water addition in an A_NA_H mechanism, forming the protonated tetrahedral intermediate. The calculated 3-^{14}C and 3,3-$^2H_2$ KIEs for the A_NA_H TS structures were well outside the range of the experimental values (Table S3). For 3-^{14}C, the $^{light}\nu^{\ddagger}/^{heavy}\nu^{\ddagger}$ values were close to unity, 1.001−1.003, because the reaction coordinate motion was dominated by nucleophile approach rather than proton transfer. The structural contributions were close to unity for either mechanism, so the calculated 3-^{14}C KIEs for the A_NA_H transition states were close to unity, 0.996−1.002, compared to the experimental value of 1.032. The experimental 3,3-$^2H_2$ KIE was 0.990, compared to the strongly inverse calculated 3,3-$^2H_2$ KIEs of 0.88−0.92 (Table S3). The inverse calculated KIEs arose largely from inverse structural contributions due to increased steric crowding and increased bond bending force constants in the sp^3-rehybridized C3 atom.[44] Thus, the mechanism was stepwise $A_H^{\ddagger}*A_N$ rather than concerted A_NA_H.

KIE Interpretation. Using the Bigeleisen−Goeppert Mayer formalism,[37,45] KIEs can be separated into the "reaction coordinate contribution" and the "structural contribution".[14] The reaction coordinate contribution is simply the ratio of reaction coordinate frequencies for the light and heavy isotopes, $^{light}\nu^{\ddagger}/^{heavy}\nu^{\ddagger}$. The structural contribution reflects the changes in structure and bond strengths between reactant and transition state. A bond becoming weaker at the transition state will give a normal structural contribution, i.e., $^{light}k/^{heavy}k > 1$, while a bond becoming stronger will give an inverse structural contribution, i.e., $^{light}k/^{heavy}k < 1$. The structural contribution is the product of the contribution from zero points energies (ZPE), which is usually the largest contributor, with further contributions from excited state vibrations (EXC) and the vibrational product (VP).[46] Finally, a tunneling correction may be applied; the Bell tunneling correction (Q_{Bell}) has been shown to be appropriate for heavy atom KIE calculations:[30,47]

$$\text{KIE} = {}^{light}\nu^{\ddagger}/{}^{heavy}\nu^{\ddagger}(\text{ZPE} \times \text{EXC} \times \text{VP})Q_{Bell} \quad (3)$$

As discussed in the context of the acid-catalyzed EPSP hydrolysis SDKIE,[17] detailed computational interpretation of primary hydron KIEs remains a challenge.[48] Thus, in the following discussion, the AroA SDKIE is analyzed qualitatively while the other KIEs are analyzed computationally.

KIE interpretation generally involves generating TS models, such as by quantum mechanical optimizations, and then calculating KIEs from the vibrational frequencies.[12,24,37,45,49] The TS model whose calculated KIEs match the experimental values is then considered the experimental TS structure. Recently, Schramm's group has modified this approach, using frequencies from constrained optimizations for IE calculations.[29,50] Strictly speaking, vibrational frequencies derived from constrained optimizations have no physical meaning, but Singleton's group has confirmed that this approach does yield reasonable calculated KIEs if applied appropriately.[30] Errors can arise if the imaginary frequencies are very small (<50i cm^{-1}) or there is more than one imaginary frequency. Finally, the imaginary frequency from the constrained optimizations must correspond to the desired reaction coordinate. Constrained TS optimizations which satisfied Singleton's criteria were used in this study in an attempt to find late TS structures with large 3-^{14}C KIEs. The match in calculated 3-^{14}C KIEs between constrained and unconstrained TS structures supports the validity of this approach (Figures 4 and S3).

3-^{14}C KIEs. The calculated 3-^{14}C and 3,3-$^2H_2$ KIEs for the small models were similar but not identical to those for the acid-catalyzed reaction because the structural and tunneling contributions are temperature dependent (Figure 3).[37,51] The calculated KIEs varied systematically as a function of the extent of proton transfer, as reflected in n_{C3-H+}. The minimum values were for balanced TS structures, where $n_{C3-H+} \approx 0.5$, and they increased for both early and late TS structures. The 3-^{14}C KIE was dominated by the reaction coordinate contribution, $^{light}\nu^{\ddagger}/^{heavy}\nu^{\ddagger}$, as the structural contribution, ZPE × EXC × VP, did not vary significantly as a function of n_{C3-H+}.

The correlation between $^{light}\nu^{\ddagger}/\ ^{heavy}\nu^{\ddagger}$ and n_{C3-H+} arises from the movement of the transferring proton, with H$^+$ being coupled with C3. Early and late TS structures had lower reaction coordinate frequencies, $\nu^{\ddagger}$, than the balanced transition states, and stronger coupling of C3 with H$^+$. Balanced transition states had higher $\nu^{\ddagger}$ values but less coupling, and $^{light}\nu^{\ddagger}/\ ^{heavy}\nu^{\ddagger}$ values were near unity (Figure 3 and Table S1). Coupling and reaction coordinate motions are described in detail in the accompanying publication.[17]

The latest computational transition state was **11-TS**, with $n_{C3-H+} = 0.77$. Strong C3 coupling with H$^+$ gave $^{light}\nu^{\ddagger}/\ ^{heavy}\nu^{\ddagger} = 1.017$ and a calculated 3-^{14}C KIE of 1.018−1.022, depending on the reactant model. (The structural contribution is determined by both the reactant and TS models, though the effect of varying the reactant model was modest.) This was significantly less than the experimental value of 1.032. However, given the trend of increasing 3-^{14}C KIE in later transition states, was it possible that an even later TS structure would have a calculated 3-^{14}C KIE that matched the experimental value? Constrained TS optimizations, with n_{C3-H+} values fixed between 0.25 and 0.95, and n_{H+-OA} values fixed as defined by eq 2, failed to find any TS structure with higher calculated 3-^{14}C KIE than **11-TS** (Figure 4). Each structure in the range of $n_{C3-H+} = 0.35-0.65$ had a single imaginary frequency corresponding to proton transfer, and the calculated 3-^{14}C KIEs were consistent with those of other models in that range. However, while the structure with $n_{C3-H+} = 0.75$ was structurally very similar to **11-TS**, the single imaginary frequency, with $\nu^{\ddagger} = 97i$ cm^{-1} was not for proton transfer, as reflected in 3-^{14}C KIE = 1.004 and $^{light}\nu^{\ddagger}/^{heavy}\nu^{\ddagger} = 1.001$ (Figure S2). Structures constrained to higher n_{C3-H+} values had multiple imaginary frequencies below 50i cm^{-1}, none of which corresponded to proton transfer. Essentially the same result was obtained with constrained TS optimizations on model **10-TS** (Figure S3).

Thus, based on the calculated 3-^{14}C KIEs, the best match to the experimental value was with early TS models. The earliest small TS model, **2-TS-scrf**, with $n_{C3-H+} = 0.26$, had a calculated 3-^{14}C KIE of 1.028, within experimental error of the observed value, 1.032 ± 0.005.

3,3-$^2H_2$ KIEs. The calculated 3,3-$^2H_2$ KIEs were insensitive to n_{C3-H+} for early transition states, but they were lower for balanced TS models and increased for $n_{C3-H+} > 0.4$ (Figure 3). Calculated 3,3-$^2H_2$ KIEs were most inverse for balanced TS structures. The reaction coordinate contributions were large and increased in late transition states, reflecting H3 coupling with H$^+$'s motion. The structural contribution was inverse, reflecting the loss of the H3 out-of-plane bending modes about the planar sp^2-hybridized C3 as it becomes sp^3-hybridized, and the bending modes become more constrained in the transition states.[44] The experimental value was close to unity, 0.990, in

the middle of the range of calculated KIEs for early transition states.

5′-^{18}O KIEs. The inverse 5′-^{18}O KIE, 0.986 ± 0.008 reflected an increase in C2−O5′ π-bonding in response to the loss of C2−C3 π-bonding and increased charge at C2. The 5′-^{18}O KIE was in the range often observed for oxacarbenium ion-like transition states in glycoside hydrolyses,[13,52] though the most relevant case would be sialic acid hydrolysis, where there is a carboxyl group adjacent to the cationic center, which had a ring ^{18}O KIE of 0.975.[53] The 5′-^{18}O KIE of 0.986 for the AroA reaction is more inverse than might be expected for an early $A_H^{\ddagger}$*A_N transition state, but it was even more inverse for the acid-catalyzed reaction, 0.978.[17] This is consistent with a later, more oxacarbenium ion-like transition state, with $n_{C3-H+} \approx 0.6$, suggesting an even more inverse 5′-^{18}O KIE for a fully developed oxacarbenium ion. It is not clear why a large inverse KIE was observed for an early transition state, but the principle of nonperfect synchronization (PNS, or transition state imbalance) may be a factor.[54] PNS predicts that rehybridizing C3 from sp^2 toward sp^3 to accept the transferring proton will cause a loss of C3−C2 π-bonding far greater than the extent of H^+-C3 bond formation, which would lead, in turn, to increased C2−O5′ π-bonding and a more inverse 5′-^{18}O KIE than the early TS structure might suggest.

Solvent Deuterium KIE. The SDKIE, 0.97, appears to be the lowest observed to date for an enol ether protonation. The smallest value previously reported, 1.3, was for intramolecularly acid-catalyzed prostacyclin hydrolysis.[39,40] A number of factors could contribute to the SDKIE, including EIEs arising from increasing carboxyl group pK_a values in D_2O:

$$SDKIE_{observed} = SDKIE_{intrinsic} \times EIE_{C1} \times EIE_{generalacid} \quad (4)$$

EIE_{C1}, the EIE from ionization of the C1 carboxyl group, will be negligible because at pH 7.5 it is already >99.9% in the more reactive carboxylate form.[10] An increasing pK_a in the general acid residue, presumably E341, could cause a significant $EIE_{general\ acid}$, depending on its pK_a. Assuming a typical ΔpK_a value of 0.45,[55] and an unperturbed glutamate pK_a of 4.5, the fraction of the reactive carboxyl form would increase 2.8-fold in D_2O, giving an $EIE_{general\ acid} = 0.35$. However, carboxyl groups in enzyme active sites can have pK_a perturbed by >5 pH units,[56] in which case, $EIE_{general\ acid} = 0.99$. Correcting $SDKIE_{observed}$ for $EIE_{general\ acid}$ implies a range of $SDKIE_{intrinsic}$ of 0.98−2.8. For acid-catalyzed EPSP hydrolysis, $SDKIE_{observed} = 6.7$ and $SDKIE_{intrinsic} = 3.1$,[17] in the range typically observed for vinyl ether hydrolyses.[39,40] Absent other contributions, the AroA-catalyzed reaction's SDKIE was less than or equal to the acid-catalyzed reaction's. Viscosity effects and ^{2}H substitution into other exchangeable sites in the protein may also affect the SDKIE, though these effects are not typically large.[57]

Computational and theoretical studies indicate that SDKIEs should be maximal for balanced transition states and lower for early and late transition states,[43,58] though plots of experimental SDKIEs versus activation energy for acid-catalyzed reactions showed the highest values for the lowest activation energies (and therefore earliest transition states).[40] Perhaps the most straightforward explanation for this apparent contradiction is that none of the acid-catalyzed reactions in the literature had sufficiently early transition states to exhibit low SDKIEs.

The small observed SDKIE for the AroA-catalyzed reaction reflects some combination of pK_a effects on the general acid catalyst, a very early transition state, and possibly other effects common in enzymatic SDKIEs.

Other KIEs. There was no correlation between n_{C3-H+} and the calculated 1-^{14}C, 2-^{14}C, or 1,1-$^{18}O_2$ KIEs (Figure S1). As discussed in the accompanying publication, this was a consequence of the structures of the "bottom half" of the models (C1, O1, C2, O5′) being more strongly determined by interactions with counterions, solvent, and acid catalysts than by n_{C3-H+}.[17] Nonetheless, comparison of the experimental 2-^{14}C and 1,1-$^{18}O_2$ KIEs between the acid- and AroA-catalyzed reactions elucidated some of AroA's catalytic strategies.

2-^{14}C and 5′-^{18}O KIEs: Evidence for an Electrostatic Sandwich. The experimental 2-^{14}C KIE for the AroA-catalyzed reaction was significantly higher than that of the acid-catalyzed reaction (1.010 ± 0.003 vs 1.003 ± 0.003) and higher than the calculated values. This implies that the decrease in C2−C3 π-bonding as the C3−H^+ bond forms was not fully compensated by increasing $n_{C2-O5'}$. This could occur if AroA stabilized the positive charge on C2, decreasing C2's demand for bonding from O5′ and C1. This was tested with **29**, which was optimized with water molecules constrained at varying distances from C2. Waters were used because carboxylate residues were too basic and deprotonated C3 during the optimization. The calculated C2 EIE increased as the C2−O distance decreased (Figure 5). Presumably anionic carboxylate oxygens in the active site would have even larger effects. The other calculated EIEs were largely unaffected, including, somewhat counterintuitively, the 5′-^{18}O EIE. Though it is difficult to quantify the effect, stabilizing a positive charge at C2 will increase the 2-^{14}C KIE, as observed experimentally. This is consistent with mutagenesis studies which showed that the carboxylate side chains of D313 and E341 form an "electrostatic sandwich" to stabilize the cationic center at C2.[18] Thus, the 2-^{14}C KIE supports the proposed role of residues D313 and E341 in acting as an electrostatic sandwich to stabilize the cation center at C2.[18] Presumably phosphate, as product (or reactant in the reverse reaction), could also help stabilize the cationic intermediate.

Evidence for a Carboxylate−Guanidinium Interaction: 1,1-$^{18}O_2$ KIE. There is a bidentate ion pair between the C1 carboxyl group and Arg386 (R386) in AroA crystal structures.[32,59] Its importance is demonstrated by a 5000-fold decrease in specific activity in the R386M mutant.[16] The experimental 1,1-$^{18}O_2$ KIE was inverse, 0.979. This reflected the reactant's C1 carboxyl group forming a tight bidentate ion pair at the transition state. In contrast, the acid-catalyzed reaction's 1,1-$^{18}O_2$ KIE of 1.001 reflected the fact that the C1 carboxyl does not experience a change in solvation in the reaction. The same trend was observed computationally, though the calculated KIEs were less inverse than the experimental value.

AroA Active Site Cluster Models. Cluster models of the AroA active site, **30-TS** and **31-TS**, were created to investigate the effects of active site residues on the TS structure (Figure 6). In particular, with the calculated KIEs from the small TS models having established an early TS structure, the question was whether including active site residues would cause a shift in the TS structure relative to the carboxylic acid-containing small models (n_{C3-H+} = 0.49−0.77, Table S1).

Both calculated transition states were earlier, with a larger shift for the more complete model: $n_{C3-H+} = 0.40$ for **30-TS** and $n_{C3-H+} = 0.24$ for **31-TS**. The calculated 3-^{14}C KIEs and $^{light}\nu^{\ddagger}/^{heavy}\nu^{\ddagger}$ values were similar to, but slightly lower than, those for small models with similar n_{C3-H+} values (Figure 3). The cluster models included the effects of the surrounding residues and allowed the full EPSP molecule to be used. This

dx.doi.org/10.1021/ja304339h | J. Am. Chem. Soc. 2012, 134, 12958−12969

gave a more realistic picture of the active site since it included the D313 and E341 side chains that form an electrostatic sandwich,[18] plus the constellation of positive charges surrounding the reactive atoms. Thus, including active site residues in the model yielded earlier TS structures than any of the carboxylic acid-containing small models, and **31-TS** was earlier even than the models with H_3O^+ as the general acid catalyst.

Two possible sources of the shift to earlier transition states can be considered: (i) a stronger general acid catalyst and (ii) cation stabilization. Computational models with a stronger acid catalyst, H_3O^+, had earlier transition states than with carboxylic acid catalysts.[17] There is no experimental evidence regarding the E341 side chain pK_a, but perturbation to be as acidic as hydronium ion is unlikely. In any case, a decreased pK_a would decrease the concentration of the active, carboxylic acid, form at physiological pH, offsetting any increase in its ability to donate protons. Thus, a perturbed E341 pK_a could affect the TS structure but is unlikely to be a dominating factor.

Better stabilization of the positive charge on the oxacarbenium ion intermediate would cause a Hammond shift to an earlier TS structure (Figure 7). The Hammond effect can be rationalized by considering that if the enzyme stabilized a positive charge, then the greatest effect would be on the cationic intermediate itself, with its full positive charge. A balanced transition state, with a charge of +0.5, would be stabilized half as much as the intermediate, and earlier transition states would be stabilized even less. The net effect would be a shift toward the earlier transition state. The large Hammond shifts in **30-TS** and **31-TS** were evidence that the charged residues in the models stabilized the oxacarbenium ion intermediate. The exact contribution to catalysis of each residue in the cluster models awaits more detailed computational studies, but the overall trend is clear.

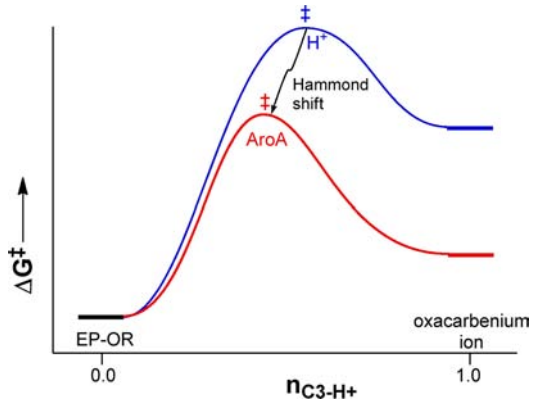

Figure 7. Hammond shift for the AroA-catalyzed reaction. n_{C3-H+} is the C3−H^+ bond order, representing the extent of reaction, with n_{C3-H+} = 0 representing the enolpyruvyl reactant (EP-OR) and n_{C3-H+} = 1 representing the oxacarbenium ion intermediate.

Enzymatic transition states reflect the interplay between the substrate's intrinsic reactivity and the enzyme's catalytic strategies. In some cases, the enzyme stabilizes essentially the same transition state as the nonenzymatic reaction, lowering the activation energy without changing the nature of the transition state. AroA did not change the transition state for C3 protonation dramatically compared to the acid-catalyzed reaction, but it did cause a shift toward an earlier transition state. This indicates that cation stabilization is a significant part of AroA's catalytic strategy, though not likely the only one.

Active Site Structure and Glu341 as a General Acid Catalyst. Conformational changes in AroA are well established experimentally. The active site closes down upon substrate binding, with residues at the lip of the active site cleft moving >20 Å.[31] This is reflected in the decrease in intrinsic Trp fluorescence upon substrate binding[19,60] and an additional decrease upon P_i binding to the AroA(D313A)·EPSP complex.[19] It is not possible to know how closely **30-TS** and **31-TS**, which were based on crystal structures, replicated the catalytically active conformation of AroA. However, the facts that the models replicated the expected Hammond shift and that the model **31-TS** gave a calculated 3-^{14}C KIE close to the experimental value argues that the model reproduced the essential features of AroA's active site. Model **30-TS**, which reproduced some of the same active site interactions in **31-TS**, had a TS structure intermediate between the small model structures and **31-TS**.

We previously identified E341 as a general acid/base catalytic residue on the basis of partitioning[16] and mutagenesis studies,[16,18] in addition to the known reaction stereo-

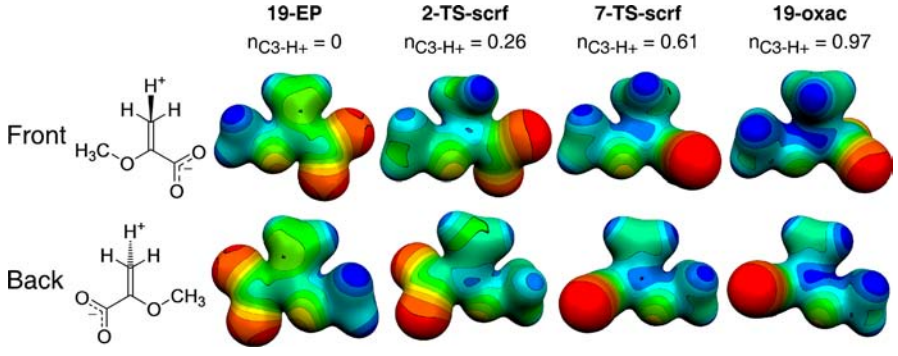

Figure 8. Electrostatic potential surfaces. The electrostatic potential surfaces from most negative (red) to most positive (blue) for structures ranging from **19-EP**, an enolpyruvyl reactant model with no proton present, through the earliest small model TS, **2-TS-scrf** (n_{C3-H+} = 0.26), to the best match to the acid-catalyzed reaction KIEs, **7-TS-scrf** (n_{C3-H+} = 0.61), and an oxacarbenium ion model, **19-oxac** (n_{C3-H+} = 0.97). The structures are from the optimized structures with all counterions, solvating waters, and acid catalysts removed to show the underlying oxacarbenium character. Wave functions were calculated at the B3PW91/6-31+G** level and mapped on the 0.02 e/b^3 isodensity surfaces. The color scale was adjusted for each structure. The range for **19-EP**, with an overall charge of −1, was −0.3 (red) to 0.04 hartree (blue). For the remaining structures, with overall charges of 0, the range was roughly −0.1 (red) to 0.25 (blue) hartree.

dx.doi.org/10.1021/ja304339h | J. Am. Chem. Soc. 2012, 134, 12958−12969

chemistry.[61] However, a consistent objection has been that E341 is too distant (3.3−3.7 Å from C3 of the THI or THI analogs) and too poorly oriented to be a catalytic residue.[7,59] A recent crystal structure of the *M. tuberculosis* AroA·S3P·PEP complex (PDB code: 2O0E) showed that a small movement in the protein backbone correctly oriented E341 Oε1 and brought it within 2.8 Å of PEP C3,[32] compared with 2.6−2.8 Å in the small TS models and 2.7 Å in **31-TS**.[62,63]

Hydrolysis versus the Normal Reaction. In this study, EPSP hydrolysis was studied rather than the normal AroA reaction because C3 protonation was cleanly irreversible, while every step in the normal reaction is reversible.[2] In the hydrolysis reaction, water adds to the EPSP cation, whereas P_i adds in the normal reverse reaction. P_i accelerates the reaction up to 10^5-fold,[19] and such a large increase could, in principle, be accompanied by a change in mechanism. There is good evidence, however, that any change would be modest. Previous studies established that EPSP cation is formed during the normal reaction when P_i is present in the active site.[10] This evidence, namely formation of the EPSP ketal side product,[64] could not distinguish between EPSP cation formation being a rare event or part of the normal reaction pathway. However, the fact that nucleophilic attack on an unactivated enolpyruvyl group is effectively impossible, with acid-catalysis accelerating the reaction >5 × 10^8-fold,[10] demonstrates that even in the presence of P_i the transition state will be highly oxacarbenium ion-like. The calculated A_NA_H transition states show that while concerted addition across the C2═C3 double bond is possible, any concerted transition state would be highly oxacarbenium ion-like, with C3 protonation almost complete and nucleophilic attack having just begun. Thus, while the normal AroA reaction is much faster than EPSP hydrolysis, changes in the TS structure will be quite modest in that AroA's demonstrated catalytic strategy of oxacarbenium ion stabilization will not be changed. The electrostatic sandwich and the carboxylate ion-pairing interaction with R386 will also be active.

Oxacarbenium Ion-like Transition State and Inhibitor Design. Though a TS structure with $n_{C3-H+} \approx 0.24$ implies only a moderately oxacarbenium ion-like transition state (Figure 8), the Hammond shift relative to the acid-catalyzed reaction implies that AroA's main catalytic strategy is cation stabilization. Good oxacarbenium ion mimics would therefore be expected to be AroA inhibitors. Glyphosate (*N*-(phosphonomethyl)glycine) binds AroA tightly, but it is not a TS mimic,[5,65] and its positive charge interacts adventitiously with E341.[31] Other cationic inhibitors have been synthesized, but none were extremely potent.[66] The ideal hypothetical inhibitor might include a planar geometry around the position of C2 and positive charge at or near that position, along with the important recognition elements from S3P, including its phosphate group, which confers 8.7 kcal/mol in binding energy.[67] Based on the increase in EPSP cation stabilization upon phosphate binding, as manifested by a 10^5-fold increase in k_{cat}, one might expect that phosphate binding should be synergistic with a sufficiently good oxacarbenium ion mimic.[10,19]

■ CONCLUSIONS

We have performed TS analysis on AroA-catalyzed EPSP hydrolysis as an analog of AroA's reverse reaction. C3 protonation was irreversible, as shown by the lack of proton exchange into EPSP during the reaction. A P_i scavenging system was developed to remove phosphate, which, though present in microscopic amounts in solution, is ubiquitous. AroA catalyzed an early transition state for proton transfer during EPSP cation formation, as reflected in the large 3-^{14}C KIE, which indicated strong coupling of C3 with the motion of the transferring proton. The solvent deuterium KIE was very small. A cluster model of AroA's active site gave an earlier transition state than small molecule models, showing that it was possible to reproduce important features of AroA's active site computationally. The 2-^{14}C KIE reflected interactions with the "electrostatic sandwich" to stabilize the positive charge at C2, and the 1,1-$^{18}O_2$ KIE reflected the bidentate ion pair formed with R386 in the active site. In stabilizing this transition state, AroA effected a large Hammond shift relative to the acid-catalyzed reaction by shifting the transition state earlier, indicating stabilization of the oxacarbenium ion intermediate.

■ ASSOCIATED CONTENT

Supporting Information

Complete citations for refs 21 and 34; calculated KIEs, reaction coordinate contributions, and calculated EIEs; imaginary frequencies for constrained models; and Cartesian coordinates for optimized active model structures. This material is available free of charge via the Internet at http://pubs.acs.org.

■ AUTHOR INFORMATION

Corresponding Author

berti@mcmaster.ca

Notes

The authors declare no competing financial interest.

[§]née Clark.

■ ACKNOWLEDGMENTS

We thank Joan Lowe-Ching for performing some of the solvent deuterium isotope effect measurements, and Paul Chindemi for $AroA_{H6}$ and S3P production. We also thank Prof. Paul Ayers (McMaster) for many helpful discussions. This work was supported by Canadian Institutes of Health Research Operating Grant MOP-64422.

■ REFERENCES

(1) Abbreviations: $A_H^{\ddagger}$*A_N, a stepwise addition mechanism with protonation being the first, rate-limiting step; A_NA_H, concerted addition mechanism; AroA, 5-enolpyruvylshikimate 3-phosphate synthase; AroK, shikimate kinase; CPCM, conductor-like polarizable continuum model; cpm, counts per min; EIE, equilibrium isotope effect; EPSP, 5-enolpyruvylshikimate 3-phosphate; EXC, excited state contribution to KIEs; G6PDH, glucose 6-phosphate dehydrogenase; KIE, kinetic isotope effect; MurA, UDP-*N*-acetylglucosamine enolpyruvyl transferase; PEP, phosphoenolpyruvate; P_i, inorganic phosphate; ppsA, phosphoenolpyruvate synthetase; S3P, shikimate 3-phosphate; SCRF, self-consistent reaction field; SDKIE, solvent deuterium kinetic isotope effect; TBAS, tetrabutylammonium sulfate; THI, tetrahedral intermediate; TS, transition state; VP, vibrational product; ZPE, zero point energy contribution to KIEs.

(2) Anderson, K. S.; Johnson, K. A. *Chem. Rev.* **1990**, *90*, 1131−1149.

(3) Roberts, F.; Roberts, C. W.; Johnson, J. J.; Kyle, D. E.; Krell, T.; Coggins, J. R.; Coombs, G. H.; Milhous, W. K.; Tzipori, S.; Ferguson, D. J.; Chakrabarti, D.; McLeod, R. *Nature* **1998**, *393*, 801−805.

(4) Priebe, G. P.; Meluleni, G. J.; Coleman, F. T.; Goldberg, J. B.; Pier, G. B. *Infect. Immun.* **2003**, *71*, 1453−1461. Stritzker, J.; Janda, J.; Schoen, C.; Taupp, M.; Pilgrim, S.; Gentschev, I.; Schreier, P.; Geginat, G.; Goebel, W. *Infect. Immun.* **2004**, *72*, 5622−5629.

(5) Steinrucken, H. C.; Amrhein, N. *Biochem. Biophys. Res. Commun.* **1980**, *94*, 1207−1212.

(6) Kahan, F. M.; Kahan, J. S.; Cassidy, P. J.; Kropp, H. *Ann. N. Y. Acad. Sci.* **1974**, *235*, 364−386.
(7) Priestman, M. A.; Healy, M. L.; Becker, A.; Alberg, D. G.; Bartlett, P. A.; Lushington, G. H.; Schonbrunn, E. *Biochemistry* **2005**, *44*, 3241−3248. Funke, T.; Healy-Fried, M. L.; Han, H.; Alberg, D. G.; Bartlett, P. A.; Schonbrunn, E. *Biochemistry* **2007**, *46*, 13344−13351.
(8) Alberg, D. G.; Lauhon, C. T.; Nyfeler, R.; Fassler, A.; Bartlett, P. A. *J. Am. Chem. Soc.* **1992**, *114*, 3535−3546. Alberg, D. G.; Bartlett, P. A. *J. Am. Chem. Soc.* **1989**, *111*, 2337−2338.
(9) Byczynski, B.; Mizyed, S.; Berti, P. J. *J. Am. Chem. Soc.* **2003**, *125*, 12541−12550.
(10) Clark, M. E.; Berti, P. J. *Biochemistry* **2007**, *46*, 1933−1940.
(11) Schramm, V. L. *Acc. Chem. Res.* **2003**, *36*, 588−596.
(12) Berti, P. J.; McCann, J. A. B. *Chem. Rev.* **2006**, *106*, 506−555.
(13) Berti, P. J.; Tanaka, K. S. E. *Adv. Phys. Org. Chem.* **2002**, *37*, 239−314.
(14) Wilson, E. B., Jr.; Decius, J. C.; Cross, P. C. *Molecular Vibrations: The Theory of Infrared and Raman Vibrational Spectroscopy*; McGraw-Hill: New York, 1955. Suhnel, J.; Schowen, R. L. In *Enzyme mechanism from isotope effects*; Cook, P. F., Ed.; CRC Press, Inc.: Boca Raton, FL, 1991; pp 3−35. Berti, P. J. *Methods Enzymol.* **1999**, *308*, 355−397.
(15) Anderson, K. S. *Arch. Biochem. Biophys.* **2005**, *433*, 47−58.
(16) Mizyed, S.; Wright, J. E. I.; Byczynski, B.; Berti, P. J. *Biochemistry* **2003**, *42*, 6986−6995.
(17) Lou, M.; Gilpin, M. E.; Burger, S. K.; Malik, A.; Gawuga, V.; Popović, V.; Capretta, A.; Berti, P. J. *J. Am. Chem. Soc.* **2012**, DOI: 10.1021/ja3043382.
(18) Berti, P. J.; Chindemi, P. *Biochemistry* **2009**, *48*, 3699−3707.
(19) Zhang, F.; Berti, P. J. *Biochemistry* **2006**, *45*, 6027−6037.
(20) Lanzetta, P. A.; Alvarez, L. J.; Reinach, P. S.; Candia, O. A. *Anal. Biochem.* **1979**, *100*, 95−97.
(21) Frisch, M. J.; et al. *Gaussian 09*; Gaussian, Inc.: Wallingford, CT, 2009.
(22) Cossi, M.; Rega, N.; Scalmani, G.; Barone, V. *J. Comput. Chem.* **2003**, *24*, 669−681. Barone, V.; Cossi, M. *J. Phys. Chem. A* **1998**, *102*, 1995−2001.
(23) Loncke, P. G.; Berti, P. J. *J. Am. Chem. Soc.* **2006**, *128*, 6132−6140.
(24) Saunders, M.; Laidig, K. E.; Wolfsberg, M. *J. Am. Chem. Soc.* **1989**, *111*, 8989−8994.
(25) In IUPAC nomenclature, proton addition is an A_H step, and nucleophile addition is A_N. A_NA_H is a concerted mechanism, with nucleophile and proton addition occurring simultaneously. An $A_H{}^*A_N$ mechanism is stepwise, with a discrete cationic intermediate (EPSP cation) that is too short-lived to diffusionally equilibrate with solvent.[26] $A_H + A_N$ indicates a stepwise mechanism where the cationic intermediate is sufficiently long-lived to diffusionally equilibrate with solvent. As discussed in the accompanying publication,[17] there is evidence that EPSP cation is too reactive to diffusionally equilibrate with solvent, making an $A_H{}^*A_N$ mechanism more likely than $A_H + A_N$. In the enzymatic reaction, EPSP cation is tightly bound by the active site, making diffusion away from the enzyme highly unlikely and favoring an $A_H{}^*A_N$ mechanism. The first step, C3 protonation, is irreversible; therefore, the mechanism is $A_H{}^{\ddagger *}A_N$.
(26) Guthrie, R. D.; Jencks, W. P. *Acc. Chem. Res.* **1989**, *22*, 343−349; *Pure Appl. Chem.* **1989**, *61*, 23−56.
(27) Pauling bond order: $n_{ij} = \exp(r_1 - r_{ij})/0.3$, where r_{ij} is the distance between atoms i and j, and r_1 is the single bond length between i and j.
(28) Luo, M.; Li, L.; Schramm, V. L. *Biochemistry* **2008**, *47*, 2565−2576. Singh, V.; Schramm, V. L. *J. Am. Chem. Soc.* **2006**, *128*, 14691−14696. Singh, V.; Luo, M.; Brown, R. L.; Norris, G. E.; Schramm, V. L. *J. Am. Chem. Soc.* **2007**, *129*, 13831−13833. Zhang, Y.; Luo, M.; Schramm, V. L. *J. Am. Chem. Soc.* **2009**, *131*, 4685−4694. Schwartz, P. A.; Vetticatt, M. J.; Schramm, V. L. *Biochemistry* **2011**, *50*, 1412−1420. Zhang, Y.; Schramm, V. L. *J. Am. Chem. Soc.* **2010**, *132*, 8787−8794.
(29) Parikh, S. L.; Schramm, V. L. *Biochemistry* **2004**, *43*, 1204−1212. Singh, V.; Lee, J. E.; Nunez, S.; Howell, P. L.; Schramm, V. L. *Biochemistry* **2005**, *44*, 11647−11659.
(30) Hirschi, J. S.; Takeya, T.; Hang, C.; Singleton, D. A. *J. Am. Chem. Soc.* **2009**, *131*, 2397−2403.
(31) Schonbrunn, E.; Eschenburg, S.; Shuttleworth, W. E.; Schloss, J. V.; Amrhein, N.; Evans, J. N. S.; Kabsch, W. *Proc. Natl. Acad. Sci. U.S.A.* **2001**, *98*, 1376−1380.
(32) Kachalova, G. S.; Burenkov, G. P.; Strizhov, N. I.; Brunning, M. G.; Bartunik, H. D. *Mycobacterium Tuberculosis Structural Proteomics Project (XMTB): Protein Data Base ID# 2O0E (to be published)*; 2008, DOI: 10.2210/pdb2o0e/pdb.
(33) Chen, V. B.; Arendall, W. B.; Headd, J. J.; Keedy, D. A.; Immormino, R. M.; Kapral, G. J.; Murray, L. W.; Richardson, J. S.; Richardson, D. C. *Acta Crystallogr., D* **2010**, *66*, 12−21.
(34) Case, D. A.; et al. AMBER 11; University of California, San Francisco: San Francisco, 2010.
(35) Bashford, D.; Case, D. A. *Annu. Rev. Phys. Chem.* **2000**, *51*, 129−152.
(36) Burger, S. K.; Ayers, P. W. *J. Chem. Phys.* **2010**, *132*, 234110.
(37) Bigeleisen, J.; Wolfsberg, M. *Adv. Chem. Phys.* **1958**, *1*, 15−76.
(38) Competitive KIEs are KIEs on k_{cat}/K_M, where the reactant is the free substrate, 33-EP (EPSP), in solution. Using the active site model 31-EP gives calculated KIEs on k_{cat}, rather than k_{cat}/K_M. The similarity of the 3-^{14}C KIEs calculated with both models (1.025 versus 1.027, respectively, for the mixed basis set models) demonstrated that the calculated KIEs were not very sensitive to the reactant molecule's environment.
(39) Chiang, Y.; Cho, M. J.; Euser, B. A.; Kresge, A. J. *J. Am. Chem. Soc.* **1986**, *108*, 4192−4196. Kresge, A. J.; Sagatys, D. S.; Chen, H. L. *J. Am. Chem. Soc.* **1977**, *99*, 7228−7233.
(40) Kresge, A. J. *Acc. Chem. Res.* **1987**, *20*, 364−370.
(41) Kohen, A.; Klinman, J. P. *Chem. Biol.* **1999**, *6*, R191−R198.
(42) Richard, J. P.; Williams, K. B.; Amyes, T. L. *J. Am. Chem. Soc.* **1999**, *121*, 8403−8404. Richard, J. P.; Jencks, W. P. *J. Am. Chem. Soc.* **1984**, *106*, 1373−1383. Richard, J. P.; Lin, S. S.; Buccigross, J. M.; Amyes, T. L. *J. Am. Chem. Soc.* **1996**, *118*, 12603−12613. Richard, J. P.; Amyes, T. L.; Lin, S. S.; O'Donoghue, A. C.; Toteva, M. M.; Tsuji, Y.; Williams, K. B. *Adv. Phys. Org. Chem.* **2000**, *35*, 67−115.
(43) Tsang, W. Y.; Richard, J. P. *J. Am. Chem. Soc.* **2009**, *131*, 13952−13962.
(44) Matsson, O.; Westaway, K. C. *Adv. Phys. Org. Chem.* **1998**, *31*, 143−248. Poirier, R. A.; Wang, Y.; Westaway, K. C. *J. Am. Chem. Soc.* **1994**, *116*, 2526−2533.
(45) Bigeleisen, J.; Goeppert Mayer, M. *J. Chem. Phys.* **1947**, *15*, 261−267.
(46) VP is the vibrational product derived from the Teller−Redlich rule: $VP = vp_{TS}/vp_{reactant}$, $vp = \Pi_i^x({}^{light}\nu/{}^{heavy}\nu)$, where $x = 3N - 7$ (TS) or $3N - 7$ (reactant), and N = the number of atoms. The contribution from mass and moments of inertia, MMI, is given by $MMI = {}^{light}\nu^{\ddagger}/{}^{heavy}\nu^{\ddagger} \times VP$.
(47) Bell, R. P. *Trans. Faraday Soc.* **1959**, *55*, 1−4.
(48) Wong, K. Y.; Richard, J. P.; Gao, J. L. *J. Am. Chem. Soc.* **2009**, *131*, 13963−13971.
(49) Schramm, V. L. *J. Biol. Chem.* **2007**, *282*, 28297−28300.
(50) Lewandowicz, A.; Schramm, V. L. *Biochemistry* **2004**, *43*, 1458−1468.
(51) Buddenbaum, W. E.; Yankwich, P. E. *J. Phys. Chem.* **1967**, *71*, 3136−3143. Stern, M. J.; Spindel, W.; Monse, E. U. *J. Chem. Phys.* **1968**, *48*, 2908−2919. Stern, M. J.; Spindel, W.; Monse, E. U. *J. Chem. Phys.* **1970**, *52*, 2022−2035.
(52) Indurugalla, D.; Bennet, A. J. *J. Am. Chem. Soc.* **2001**, *123*, 10889−10898. Berti, P. J.; Blanke, S. R.; Schramm, V. L. *J. Am. Chem. Soc.* **1997**, *119*, 12079−12088. Berti, P. J.; Schramm, V. L. *J. Am. Chem. Soc.* **1997**, *119*, 12069−12078.
(53) Chan, J.; Lewis, A. R.; Gilbert, M.; Karwaski, M. F.; Bennet, A. J. *Nat. Chem. Biol.* **2010**, *6*, 405−407.
(54) Bernasconi, C. F. *Acc. Chem. Res.* **1992**, *25*, 9−16. Bernasconi, C. F. *Adv. Phys. Org. Chem.* **1992**, *27*, 119−238.
(55) Bell, R. P.; Kuhn, A. T. *Trans. Faraday Soc.* **1963**, *59*, 1789−1793.
(56) Harris, T. K.; Turner, G. J. *IUBMB Life* **2002**, *53*, 85−98.

(57) Quinn, D. M.; Sutton, L. D. In *Enzyme mechanism from isotope effects*; Cook, P. F., Ed.; CRC Press, Inc.: Boca Raton, FL, 1991; pp 73−126. Karsten, W. E.; Lai, C.-J.; Cook, P. F. *J. Am. Chem. Soc.* **1995**, *117*, 5914−5918. Schowen, R. L. In *Isotope Effects In Chemistry and Biology*; Kohen, A.; Limbach, H. H., Eds.; CRC Press: Boca Raton, 2005; p 765−792.
(58) Kiefer, P. M.; Hynes, J. T. *J. Phys. Chem. A* **2003**, *107*, 9022−9039. Bell, R. P. *The Proton in Chemistry*, 2nd ed.; Cornell University Press: Ithaca, NY, 1973.
(59) Eschenburg, S.; Kabsch, W.; Healy, M. L.; Schonbrunn, E. *J. Biol. Chem.* **2003**, *278*, 49215−49222. Park, H.; Hilsenbeck, J. L.; Kim, H. J.; Shuttleworth, W. A.; Park, Y. H.; Evans, J. N.; Kang, C. *Mol. Microbiol.* **2004**, *51*, 963−971.
(60) Anderson, K. S.; Sikorski, J. A.; Johnson, K. A. *Biochemistry* **1988**, *27*, 1604−1610.
(61) Grimshaw, C. E.; Sogo, S. G.; Copley, S. D.; Knowles, J. R. *J. Am. Chem. Soc.* **1984**, *106*, 2699−2700. Lee, J. J.; Asano, Y.; Shieh, T.-L.; Spreafico, F.; Lee, K.; Floss, H. G. *J. Am. Chem. Soc.* **1984**, *106*, 3367−3368. Kim, D. H.; Tucker-Kellogg, G. W.; Lees, W. J.; Walsh, C. T. *Biochemistry* **1996**, *35*, 5435−5440. Skarzynski, T.; Kim, D. H.; Lees, W. J.; Walsh, C. T.; Duncan, K. *Biochemistry* **1998**, *37*, 2572−2577. Kim, D. H.; Lees, W. J.; Walsh, C. T. *J. Am. Chem. Soc.* **1995**, *117*, 6380−6381. Lees, W. J.; Walsh, C. T. *J. Am. Chem. Soc.* **1995**, *117*, 7329−7337.
(62) Given the close proximity of the D313 and E341 carboxylate groups to C2 of the EPSP cation intermediate, the question arises whether one or both could add to the intermediate, forming a transient covalent intermediate. This occurs in the homologous enzyme MurA, where a Cys residue forms a transient covalent hemithioketal adduct with PEP.[63] Such a covalent adduct is indeed possible, but because it would occur after the first irreversible step, it would not be observable in the experimental KIEs and would not affect the transition state for EPSP cation formation.
(63) Brown, E. D.; Marquardt, J. L.; Lee, J. P.; Walsh, C. T.; Anderson, K. S. *Biochemistry* **1994**, *33*, 10638−10645.
(64) Leo, G. C.; Sikorski, J. A.; Sammons, R. D. *J. Am. Chem. Soc.* **1990**, *112*, 1653−1654.
(65) Sammons, R. D.; Gruys, K. J.; Anderson, K. S.; Johnson, K. A.; Sikorski, J. A. *Biochemistry* **1995**, *34*, 6433−6440. Sikorski, J. A.; Gruys, K. J. *Acc. Chem. Res.* **1997**, *30*, 2−8.
(66) Marzabadi, M. R.; Gruys, K. J.; Pansegrau, P. D.; Walker, M. C.; Yuen, H. K.; Sikorski, J. A. *Biochemistry* **1996**, *35*, 4199−4210. Pansegrau, P. D.; Anderson, K. S.; Widlanski, T.; Ream, J. E.; Sammons, R. D.; Sikorski, J. A.; Knowles, J. R. *Tetrahedron Lett.* **1991**, *32*, 2589−2592. Marzabadi, M. R.; Font, J. L.; Gruys, K. J.; Pansegrau, P. D.; Sikorski, J. A. *Bioorg. Med. Chem. Lett.* **1992**, *2*, 1435−1440.
(67) Gruys, K. J.; Walker, M. C.; Sikorski, J. A. *Biochemistry* **1992**, *31*, 5534−5544.